SCIENCE CHINA
Physics, Mechanics & Astronomy

• Article •

January 2015 Vol. 58 No. 1: 014701
doi: 10.1007/s11433-014-5440-2

Investigation on transonic flutter active auppression with CFD-Based ROMs

NIE XueYuan*, YANG GuoWei & ZHANG MingFeng

Key Laboratory for Mechanics in Fluid Solid Coupling Systems, Institute of Mechanics, Chinese Academy of Sciences, Beijing 100190, China

Received April 16, 2013; accepted October 12, 2013; published online June 20, 2014

The calculation of accurate unsteady aerodynamic forces is critical in the analysis of aeroelastic problems, however the efficiency is low because of high computational costs of the computational fluid dynamics (CFD) portion. Additionally, direct integrated CFD and computational structural dynamics (CSD) technique is unsuitable for the analysis of ASE and the flutter active suppression in state-space form. A reduced-order model (ROM) based on Volterra series was developed using CFD calculation and used to predict the flutter coupled with the structure. The closed-loop control systems designed by the sliding mode control (SMC) and linear quadratic Gaussian (LQG) control were constructed with ROM/CSD to suppress the AGARD 445.6 wing flutter. The detailed implementation of the two control approaches is presented, and the flutter suppression effectiveness is discussed and compared. The results indicate that SMC method can make the controlled object response decay to the stable equilibrium more rapidly and has better control effects than the LQG control.

reduced order model, aeroelasticity, linear quadratic Gaussian control, sliding mode control, active flutter suppression

PACS number(s): 02.62.Cb, 47.40.Hg, 45.30.+s, 02.60.Pn

Citation: Nie X Y, Yang G W, Zhang M F. Investigation on transonic flutter active auppression with CFD-Based ROMs. Sci China-Phys Mech Astron, 2015, 58: 014701, doi: 10.1007/s11433-014-5440-2

1 Introduction

Based on the coupled CFD/CSD method in time domain, the calculation of unsteady aerodynamic forces has been widely applied in investigation of vehicles nonlinear aeroelastic problems [1–5]. However, it is difficult to extend the method to the application of such things as multidisciplinary optimization design, aeroservoelastic analysis and flutter active suppression, because the method is time-consuming in flow calculation and possesses a large number of degrees of freedom. Therefore, many researchers have adopted alternative unsteady aerodynamic computational methods. Among them, the rational function approximation (RFA) techniques are usually used to depict the aerodynamic forces. RFA techniques transform the linearized generalized aerodynamic forces (GAFs) in frequency-domain into the state-space form in time domain, which is suitable for the use of modern control theory and optimization. The RFA techniques cannot be used to calculate nonlinear unsteady aerodynamic forces such as in transonic or large attack angles conditions. CFD-based reduced order models (ROM) has been developed in the past 20 years. ROMs can map the large-scaled system to small-scaled one retaining the model's high fidelity, which is used to denote the degree to which a model captures the interesting physical phenomenon. ROMs are modeled with the data calculated by the direct time coupled CFD/CSD and can reflect the essential characteristics of the physical process.

At present, there are three types of methods to model ROMs. The first is based on system identification theory and construct ROMs by the input excitations and output responses of CFD/CSD coupled system, such as ARMA [6],

*Corresponding author (email: niexueyuan@imech.ac.cn)

Volterra series models [7] and neural networked models. The second is based on proper orthogonal decomposition (POD) [8] to obtain the primary flow modes to reduce the order of fluid discrete matrix, such as POD. The third is harmonic balance (HB) [9] method which is used in frequency domain to analyze nonlinear aeroelastic problems.

Flutter is a typical aeroelastic dynamic unstable phenomenon. Active flutter suppression (AFS) designs feedback control laws to ensure that the unstable open-loop system is stable. The controlled object determines the design of the controller. In the last several decades, AFS control algorithms were developed according to the transfer function of the controlled object in frequency domain [10–12]. With the development of modern flight vehicles, the transfer function which only reflects the relationship between input and output signals cannot meet the requirements of control design. The state-space models, which not only indicate the internal characteristics of the system but also dispose of multi-input and multi-output system, have become the primary trend to investigate the aeroservoelastic problems and to suppress the flutter coupled with modern control theory. Linear quadratic Gaussian control method and linear quadratic regulator control method are commonly used in AFS [13–16]. Yang et al. [17] and Kim et al. [18,19] used the sliding mode control (SMC) method for the aeroelastic control of a two-dimensional airfoil.

Herein we develop a CFD-based unsteady aerodynamic forces state-space model to accelerate aeroelastic analysis, and to design the SMC control law for the flutter suppression of the AGARD445.6 wing in addition to LQG. The results indicate that the ROM can replace the CFD calculation accurately and the designed control laws for the coupled ROM/CSD system can effectively suppress flutter.

Herein we introduce the Volterra theory, followed by the CFD-based step response technique. The Eigensystem Realization Algorithm (ERA) [20], which transforms the step responses into state-space form, that is, unsteady aerodynamic forces model, is then described. The aeroelastic state-space model is generated by the coupling the CFD-based ROM with the structure state-space model. As the example of AGARD445.6 aeroelastic wing, the aeroelastic responses can be rapidly predicted with the root locus method of the aeroelastic system's characteristic matrix or using direct time-marching solutions. Lastly, the control laws are designed successfully in MATLAB/SIMULINK environment with two state feedback methods for the active flutter suppression, which are the SMC and linear quadratic Gaussian method (LQG).

2 CFD-based ROM with Volterra series

2.1 Volterra theory

Volterra series was propounded by mathematician Volterra in 1880 as the extention of Taylor series [21]. The basic premise is that any nonlinear system can be modeled as an infinite sum of multidimensional convolution integrals of increasing order. The infinite sum, presented herein is the discrete-time form given below:

$$\begin{aligned} y[n] = h_0 &+ \sum_{k=0}^{n} h_1[n-k]u[k] \\ &+ \sum_{k_1=0}^{n}\sum_{k_2=0}^{n} h_2[n-k_1, n-k_2]u[k_1]u[k_2] \\ &+ \cdots + \sum_{k_1=0}^{n}\sum_{k_2=0}^{n}\cdots \\ &\times \sum_{k_m=0}^{n} h_m[n-k_1, n-k_2, \cdots, n-k_m]u[k_1]u[k_2] \\ &\cdots u[k_m] + \cdots, \end{aligned} \tag{1}$$

where $y[n]$ is the response of the nonlinear system to $u[n]$, for an arbitrary input, n denotes discrete time, $h_m[n-k_1, n-k_2, \cdots, n-k_m]$ is the mth order Volterra kernel. Eq. (1) shows that the responses of the nonlinear system to arbitrary inputs can be predicted once the Volterra kernels are identified. To obtain all kernels is important to successfully model a nonlinear system in Volterra series representation.

As the CFD/CSD techniques developed, Volterra series has been used in modeling unsteady aerodynamic forces. The unsteady fluid flows described by Euler equations and Navier-Stokes equations in aeroelastic problems can be assumed as weakly nonlinear systems [22,23]. A weakly nonlinear system is well defined by the first two orders kernels of the Volterra series. The truncated second-order Volterra series, which represents CFD model, is given below:

$$\begin{aligned} y[n] = h_0 &+ \sum_{k=0}^{n} h_1[n-k]u[k] \\ &+ \sum_{k_1=0}^{n}\sum_{k_2=0}^{n} h_2[n-k_1, n-k_2]u[k_1]u[k_2]. \end{aligned} \tag{2}$$

Silva [22] firstly identified Volterra kernels and constructed CFD-based ROM with the responses of impulse excitation. Raveh [24] found that the amplitudes and time steps of excitations influenced greatly on impulse response method and at times was unable to accurately represent the unsteady characteristics of the nonlinear system. The step responses approach is suggested to use. Herein the step response is adopted to identify Volterra kernels.

Define discrete-time step signal as:

$$\xi[n] = \begin{cases} \xi_0, & n \geqslant 0, \\ 0.0, & n < 0. \end{cases}$$

Exert this signal as input to eq. (2) and by negating steady value h_0, the responses of step signals can be written in the following:

$$s[n]=\xi_0\sum_{k=0}^{n}h_1[n-k]+{\xi_0}^2\sum_{k_1=0}^{n}\sum_{k_2=0}^{n}h_2[n-k_1,n-k_2], \tag{3}$$

where $s[n]$ represents the responses of step input, it includes the second-order kernel which is far smaller than the first-order one. If the second-order kernel neglected, the following approximate relation can be obtained:

$$s[n]=\xi_0\sum_{k=0}^{n}h_1[n-k]. \tag{4}$$

Then the first-order Volterra kernel is derived from eq. (4) such that

$$h[n]=\begin{cases}s[0]/\xi_0, & n=0,\\ \big(s[n]-s[n-1]\big)/\xi_0, & n\geqslant 1.\end{cases} \tag{5}$$

For this first-order kernel contains second-order kernel component, eq. (5) can then reflect certain nonlinear behavior.

2.2 ROMs of unsteady aerodynamic forces

The state-space model was constructed by the Eigensystem realization algorithm (ERA) using Markov parameters which compose the Hankel matrix with discrete-time impulse responses. Via Singular Value Decomposition (SVD), the state-space model matrix can be computed.

The CFD-based ROM via ERA approach is determined as below:

$$\begin{aligned}\boldsymbol{x}_{\mathrm{a}}(n+1)&=A_{\mathrm{a}}\boldsymbol{x}_{\mathrm{a}}(n)+B_{\mathrm{a}}\xi(n),\\ \boldsymbol{y}_{\mathrm{a}}(n)&=C_{\mathrm{a}}\boldsymbol{x}_{\mathrm{a}}(n)+D_{\mathrm{a}}\xi(n),\end{aligned} \tag{6}$$

where $\boldsymbol{x}_{\mathrm{a}}(n)$ is GAFs state vector, $\xi(n)$ is the generalized structure displacement and $y_{\mathrm{a}}(n)$ is GAF. The Markov parameters of the model can be deduced from eq. (3) expressed as:

$$y_{\mathrm{a}}(n)=\big(s(n)-s(n-1)\big)\big/\xi_0=C_{\mathrm{a}}A_{\mathrm{a}}^{n-1}B_{\mathrm{a}},\quad (n\geqslant 1). \tag{7}$$

Assumed Markov parameters are ($L\times P$) matrix, Hankle matrix is constructed in the following form:

$$\boldsymbol{H}(k-1)=\begin{bmatrix}y_{\mathrm{a}}(n) & y_{\mathrm{a}}(n+1) & \cdots & y_{\mathrm{a}}(n+\beta-1)\\ y_{\mathrm{a}}(n+1) & y_{\mathrm{a}}(n+2) & \cdots & y_{\mathrm{a}}(n+\beta)\\ \vdots & & & \vdots\\ y_{\mathrm{a}}(n+\alpha-1) & y_{\mathrm{a}}(n+\alpha) & \cdots & y_{\mathrm{a}}(n+\alpha+\beta-2)\end{bmatrix}, \tag{8}$$

where α,β are selected integers.

Apply SVD to $\boldsymbol{H}(0)$,

$$\boldsymbol{H}(0)=\boldsymbol{U}^{\mathrm{T}}\sum\boldsymbol{V}, \tag{9}$$

where $\boldsymbol{U},\sum,\boldsymbol{V}$ are the left singular value vector, the singular value matrix and the right singular value vector, respectively.

Let

$$\boldsymbol{E}_L^{\mathrm{T}}=\begin{bmatrix}I_L & 0_L & \cdots & 0_L\end{bmatrix}_{L\times L\alpha},$$
$$\boldsymbol{E}_P^{\mathrm{T}}=\begin{bmatrix}I_P & 0_P & \cdots & 0_P\end{bmatrix}_{P\times P\beta},$$

each coefficient matrix of eq. (6) is acquired respectively as:

$$\begin{aligned}\boldsymbol{A}_{\mathrm{a}}&=\sum^{-\frac{1}{2}}\boldsymbol{U}\boldsymbol{H}(1)\boldsymbol{V}^{\mathrm{T}}\sum^{-\frac{1}{2}},\\ \boldsymbol{B}_{\mathrm{a}}&=\sum^{\frac{1}{2}}\boldsymbol{V}\boldsymbol{E}_P,\\ \boldsymbol{C}_{\mathrm{a}}&=\boldsymbol{E}_L^{\mathrm{T}}\boldsymbol{U}^{\mathrm{T}}\sum^{\frac{1}{2}},\\ D_{\mathrm{a}}&=y_{\mathrm{a}}(0)=s(0).\end{aligned} \tag{10}$$

Currently, all model parameters of Volterra-based ROM have been identified and the model of unsteady aerodynamic forces has been generated.

3 Aeroelastic state-space model

For flutter analysis, modal equations are used to calculate the structural deformation under GAFs [25]. For each mode *i*, the mass-normalized modal dynamic equation is written in the following form:

$$\begin{aligned}&\ddot{\eta}_i(t)+2\zeta_i\omega_i\dot{\eta}_i(t)+\omega_i^2\eta_i(t)=f_i(t),\ i=1,\cdots N,\\ &d(x,y,z,t)=\sum_{i=1}^{N}\eta_i(t)\{\varphi_i(x,y,z)\},\\ &f_i(t)=F(x,y,z,t)\{\varphi_i(x,y,z)\},\end{aligned} \tag{11}$$

where $\omega_i,\{\varphi_i(x,y,z)\}$ are the *i*th structure modal frequency and modal shape, respectively. N represents the number of modal shapes. $f_i(t)$ is the *i*th GAFs and η_i is the *i*th generalized structure displacement. $d(x,y,z,t)$ is the structure physical displacement and $F(x,y,z,t)$ is aerodynamic force.

Convert the first equation in eq. (11) into the state-space form as:

$$\begin{cases}\dot{x}_{\mathrm{s}}(t)=A_{\mathrm{s}}x_{\mathrm{s}}(t)+qB_{\mathrm{s}}y_{\mathrm{a}}(t),\\ \xi(t)=C_{\mathrm{s}}x_{\mathrm{s}}(t)+D_{\mathrm{s}}y_{\mathrm{a}}(t),\end{cases} \tag{12}$$

where q is dynamic pressure,

$$x_{\mathrm{s}}(t)=\begin{bmatrix}\eta_1(t) & \cdots & \eta_N(t) & \dot{\eta}_1(t) & \cdots & \dot{\eta}_N(t)\end{bmatrix}^{\mathrm{T}},$$

$$y_{\mathrm{a}}(t)=\begin{bmatrix}0 & \cdots & 0 & f_1(t) & \cdots & f_N(t)\end{bmatrix}^{\mathrm{T}},$$

$$A_{\mathrm{s}}=\begin{bmatrix} 0 & \cdots & 0 & 1 & \cdots & 0 \\ & \ddots & & & \ddots & \\ 0 & \cdots & 0 & 0 & \cdots & 1 \\ -\omega_1^{\,2} & & & -2\zeta_1\omega_1 & & \\ & & -\omega_N^{\,2} & & & -2\zeta_N\omega_N \end{bmatrix},$$

$$B_{\mathrm{s}}=\begin{bmatrix} 0 \\ \vdots \\ 0 \\ 1 \\ \vdots \\ 1 \end{bmatrix},\quad C_{\mathrm{s}}=\begin{bmatrix} \mathrm{I}_{N\times N} & \\ & 0_{N\times N} \end{bmatrix},\quad D_{\mathrm{s}}=[0].$$

Eq. (12) is discretized with zero-order holder and the discrete-time structure state-space model is thus obtained:

$$\begin{cases} x_{\mathrm{s}}(n+1)=A_{\mathrm{s}}'x_{\mathrm{s}}(n)+qB_{\mathrm{s}}'y_{\mathrm{a}}(n), \\ \xi(n)=C_{\mathrm{s}}'x_{\mathrm{s}}(n)+D_{\mathrm{s}}'y_{\mathrm{a}}(n), \end{cases} \tag{13}$$

where

$$A_{\mathrm{s}}'=\mathrm{e}^{A_{\mathrm{s}}T},B_{\mathrm{s}}'=\left(\int_0^T\mathrm{e}^{A_{\mathrm{s}}t}\mathrm{d}t\right)B_{\mathrm{s}},C_{\mathrm{s}}'=C_{\mathrm{s}},D_{\mathrm{s}}'=D_{\mathrm{s}}.$$

Here T is the sampling time, the model input $y_{\mathrm{a}}(n)$ is GAFs and the output $\xi(n)$ is the generalized structure displacement.

The discretized structure model eq. (13) can be combined with eq. (6) to constitute the aeroelastic state-space model. It is given by eq. (14):

$$\begin{bmatrix} x_{\mathrm{s}}(n+1) \\ x_{\mathrm{a}}(n+1) \end{bmatrix}=\begin{bmatrix} A_{\mathrm{s}}'+qB_{\mathrm{s}}'D_{\mathrm{a}}C_{\mathrm{s}} & qB_{\mathrm{s}}'C_{\mathrm{a}} \\ B_{\mathrm{a}}C_{\mathrm{s}} & A_{\mathrm{a}} \end{bmatrix}\begin{bmatrix} x_{\mathrm{s}}(n) \\ x_{\mathrm{a}}(n) \end{bmatrix},$$
$$\xi(n)=\begin{bmatrix} C_{\mathrm{s}} & 0 \end{bmatrix}\begin{bmatrix} x_{\mathrm{s}}(n) \\ x_{\mathrm{a}}(n) \end{bmatrix}. \tag{14}$$

For aeroelastic model eq. (14), the flutter dynamic pressure and frequency can be determined by the root locus of the characteristic matrix or direct time-marching method.

As compared with the direct CFD/CSD solution [14], ROM can improve highly the computational efficiency, since only several hundreds of CFD calculation runs are needed for each input signal of structural modes. It is more important that the aeroelastic model ROM-based are readily apprant to integrate the controller into the open-loop system to form the closed-loop system, so that the aeroservoelasticity and the flutter active suppression can be investigated.

4 Flutter analysis

In this paper, the aeroelastic standard model of AGARD 445.6 wing is used for the flutter analysis. The wing is a 45° swept-back wing with a NACA 65A004 airfoil section, panel aspect ratio of 1.65, and a taper ratio of 0.6576. The first four structural modal frequencies are 9.60, 38.2, 48.35, and 91.54 Hz whose additional detail parameters can be referred elsewhere [26]. Here, the Mach number is taken as 0.96, and initial attack angle is 0°.

To build Volterra-based ROM, firstly using CFD code based on Navier-Stokes Solver, each mode is individually excited to obtain the responses of all the modes to be used to identify Volterra kernel. Herein, the first four modes are used and the step signals with amplitude 2×10^{-5} are selected. Take time step size as 8.678×10^{-5} s, with the corresponding dimensionless time as 0.05. The whole process is depicted in Figure 1. Secondly, based on the calculated GAFs, that is, step responses, Volterra kernels are identified with eq. (5). The results are shown in Figure 2, where A_{ij} represents jth aerodynamic force response to ith structure modal deformation.

Then, with the Volterra kernels and ERA approach, the unsteady aerodynamic forces model can be determined. At last, to verify the CFD-based ROM, CFD/CSD simulation is adopted to validate the ROM method. In Figure 3, at given dynamic pressure $61.3lbf\,/\,ft^2$ and impulse input, GAFs computed by ROM/CSD and by CFD/CSD coupled calculation are compared.

A fit parameter was defined as:

$$\eta=1-\sqrt{\frac{\sum_{i=1}^{n}(F_{\mathrm{A}i}-\hat{F}_{\mathrm{A}i})^2}{\sum_{i=1}^{n}F_{\mathrm{A}i}^{\,2}}},$$

where F_{A} and $\hat{F}_{\mathrm{A}}$ are the vectors of measured and simulated aerodynamic force, respectively. Table 1 presents comparison of the fit parameters of the four modal responses calculated by CFD/CSD and ROM/CSD. It can be seen that CFD-based ROM can predict unsteady aerodynamic forces consistently.

To verify the aeroelastic state-space models, we calculate

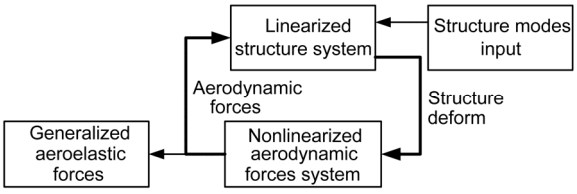

Figure 1 Calculation of GAFs for identifying Volterra kernels.

Table 1 Fitting degrees of modal generalized displacement of direct CFD and Volterra-based ROM methods

Modal output	1st	2nd	3rd	4th
η (%)	99.58	99.72	99.81	97.44

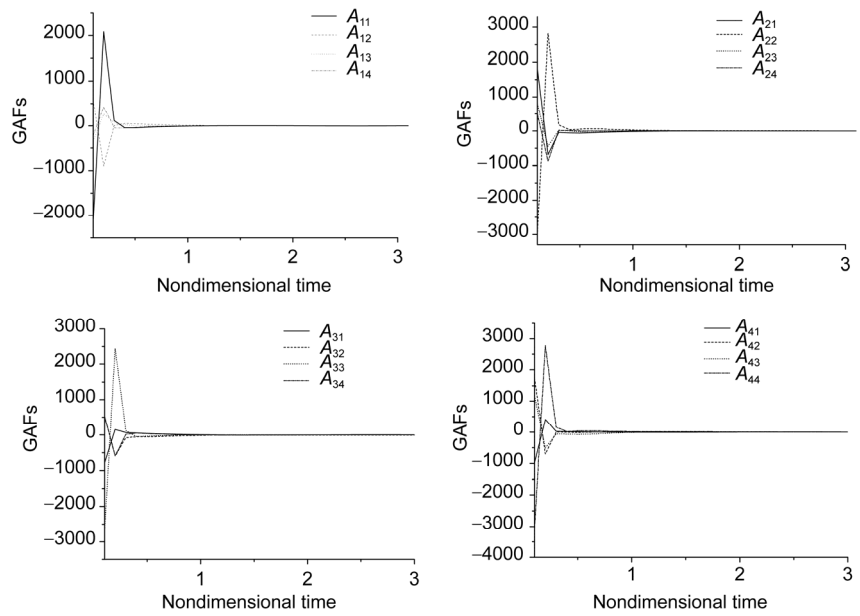

Figure 2 Volterra kernels with step excitation.

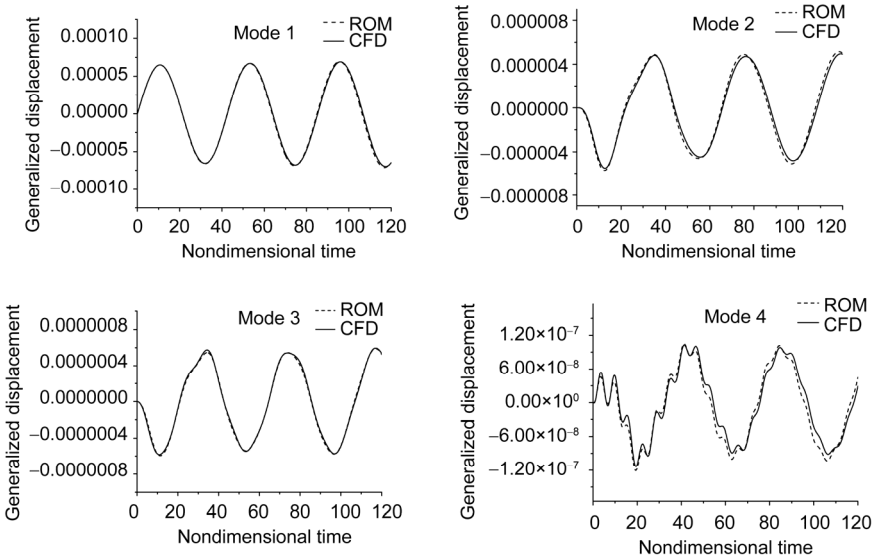

Figure 3 Comparison of generalized modal displacement with direct CFD/CSD and Volterra-based ROM/CSD.

the structure responses to zero dynamic pressure. In this instance, they are actually free vibrations. Figure 4 depicts the generalized structure displacement responses in frequency domain without structure damp and the first four structure natural frequencies are 9.6, 38.2, 48.4 and 91.5 Hz, respectively.

Combining the ROM of aerodynamic forces with linear structure model, the aeroelastic analysis model is obtained. By changing dynamic pressure, we can acquire the distribution of characteristic roots of the aeroelastic system in unit circle. According to Lyapunov stability criteria, the corresponding flutter dynamic pressure is $55.78 lbf/ft^2$ as shown in Figure 5. Alternatively we can directly solve aeroelastic state-space equation in time domain and get the time histories of generalized structure displacement at different dynamic pressures. Figure 6 gives the comparison of the generalized structure displacements between CFD/CSD and CFD-based ROM. From Figure 6 it appears that the CFD-based ROM does not capture the response of the fourth mode to the excitation accurately. However, the amplitude of the response is one to two orders of magnitude smaller than the amplitudes of the other modes GAFs to the same excitation. Overall the GAF ROM appears to be a good representation of the behavior of the system. The

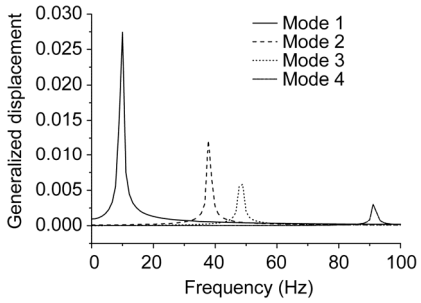

Figure 4 Free vibration of the structure.

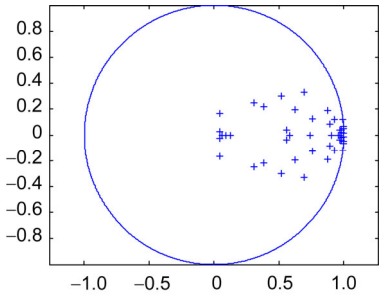

Figure 5 (Color online) Characteristic roots distribution at dynamic pressure of 55.78*lfb*/*ft*^{2}.

flutter dynamic pressure is 55.78*lfb*/*ft*^{2}, which is similar to the result of eigenvalues method.

By applying Fourier transformation to the generalized structure displacement in time domain, we can obtain the flutter frequency of 13.826 Hz at Mach number of 0.96, which agrees well with the experiment result of 13.894 Hz. The flutter is the coupling result of the first with the third mode motions of the structure.

5 Active flutter suppression

5.1 Closed-loop control System

To suppress flutter, it is necessary to introduce the controller and the actuator into the aeroelastic system to form the closed-loop system. Herein, with the assumption of structural modes unchanged, we induce the control surface located at 20% chordwise position from tailing edge as the actuator. Followed by the control instruction, the control surface deflects to generate additional unsteady aerodynamic forces to realize the flutter active suppression. Thus the unsteady aerodynamic forces for the structure can be divided into two parts, one from the elastic wing and the other from the control surface deflection [11]. Consequently, eq. (14) can be rewritten as:

$$\begin{aligned} x_o(n+1) &= A_o x_o(n) + B_o y_c(n), \\ y_o(n) &= C_o x_o(n), \end{aligned} \tag{14'}$$

where

$$A_o = \begin{bmatrix} A_s' + qB_s' D_a C_s & qB_s' C_a \\ B_a C_s & A_a \end{bmatrix},$$

$$B_o = \begin{bmatrix} B_s' \\ 0 \end{bmatrix}, \quad C_o = \begin{bmatrix} C_s & 0 \end{bmatrix}, \quad x_o(n) = \begin{bmatrix} x_s(n) \\ x_a(n) \end{bmatrix}.$$

Similarly, the ROM of unsteady aerodynamic forces for

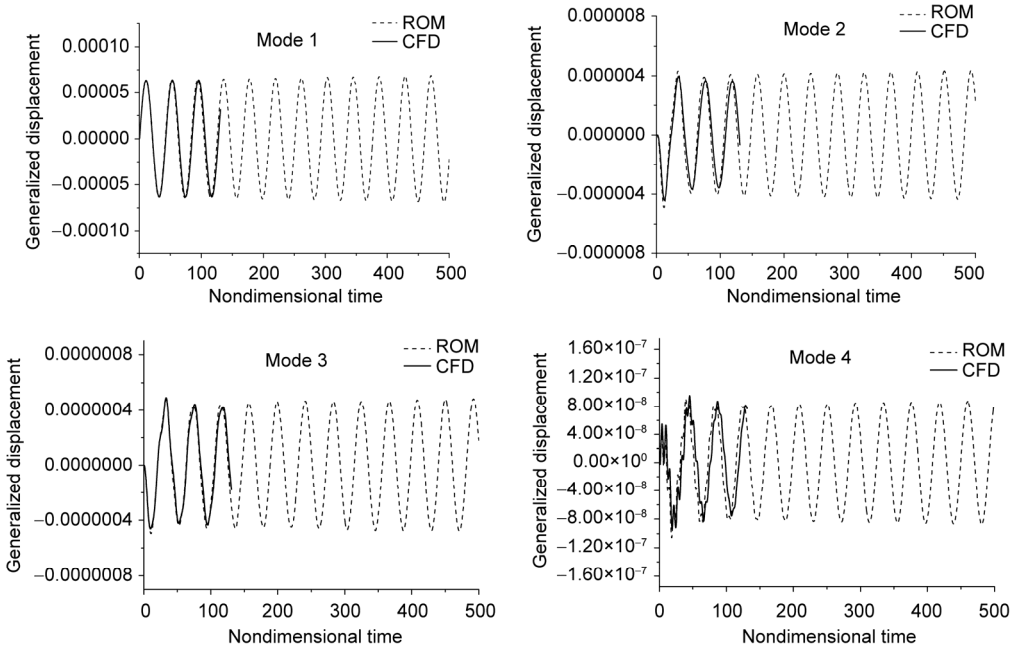

Figure 6 First four modes generalized displacement at dynamic pressure of 55.78*lfb*/*ft*^{2}.

the control surface in state-space form can also be built as following:

$$\begin{cases} x_{\mathrm{c}}(n+1) = A_{\mathrm{c}} x_{\mathrm{c}}(n) + B_{\mathrm{c}}\beta(n), \\ y_{\mathrm{c}}(n) = C_{\mathrm{c}} x_{\mathrm{c}}(n) + D_{\mathrm{c}}\beta(n), \end{cases} \tag{15}$$

where β is the deflection angle of the control surface, y_{c} is the unsteady aerodynamic forces produced by the control surface deflection.

Substitute eq. (14') into eq. (15) to form the generalize controlled object model, namely, the open-loop aeroelastic model

$$\begin{cases} x_{\mathrm{ase}}(n+1) = A_{\mathrm{ase}} x_{\mathrm{ase}}(n) + B_{\mathrm{ase}}\beta(n), \\ y_{\mathrm{ase}}(n) = C_{\mathrm{ase}} x_{\mathrm{ase}}(n), \end{cases} \tag{16}$$

where

$$A_{\mathrm{ase}} = \begin{bmatrix} A_o & qB_oC_{\mathrm{c}} \\ 0 & A_{\mathrm{c}} \end{bmatrix}, \quad B_{\mathrm{ase}} = \begin{bmatrix} B_oD_{\mathrm{c}} \\ B_{\mathrm{c}} \end{bmatrix},$$

$$C_{\mathrm{ase}} = \begin{bmatrix} C_o & 0 \end{bmatrix}, \quad x_{\mathrm{ase}}(n) = \begin{bmatrix} x_o(n) \\ x_{\mathrm{c}}(n) \end{bmatrix}.$$

The ultimate goal of active control of aeroelastic problem is to ensure that the generalized structure displacement vector $\xi(n)$ with time is inclined to equilibrium point, that is, $\lim_{n\to\infty}\|\xi(n)-c\|=0$ (c is an equilibrium point of the system) by using control law design. In other words, the controller ensures that the controlled object achieves asymptotical stability under Lyapunov meaning.

The whole closed-loop system is depicted by Figure 7.

5.2 Control laws design

The function of a controller is to form the closed-loop system to stabilize the unstable open-loop object or improve the dynamic performance of the controlled object by changing the distribution of zeros and poles of the controlled object. In the modern control theory, the state-space equations are used to represent the objects with inner state vectors, so that the controller can use the state vectors feedback as well as output signals. In the paper, the SMC method and the linear quadratic Gaussian (LQG) optimal method are used to suppress the flutter.

SMC is a nonlinear control strategy. By designing a group of sliding mode surfaces in phase space and the corresponding switching control functions, SMC can enforce all the states of the controlled object to move towards the sliding mode surfaces and to make the controlled system asymptotically stable.

The general discrete-time controlled system is as follows:

$$\begin{cases} x(n+1) = Gx(n) + Hu(n), \\ y(n) = Cx(n), \end{cases} \tag{17}$$

where $x \in R^n$, $u \in R^m$, $y \in R^l$, $l \leqslant m \leqslant n$.

It is important for SMC to determine m sliding surface functions $\sigma_i = S_i x$ ($i=1,\cdots m$) and their corresponding m switching control functions

$$u_i(n) = \begin{cases} u_i^+(x) & \sigma_i > 0, \\ u_i^-(x) & \sigma_i < 0, \end{cases} \quad (i=1,\cdots m). \tag{18}$$

Control block diagram of SMC algorithm is shown in Figure 8.

Previously, we have obtained the open-loop flutter dynamic pressure of $55.78 lbf/ft^2$ with ROM/CSD coupling analysis of the system. The simulation was set for dynamic pressure of $85 lbf/ft^2$. The first four modes generalized displacement in open-loop system is unstable, which are shown in Figure 9. Flutter occurs.

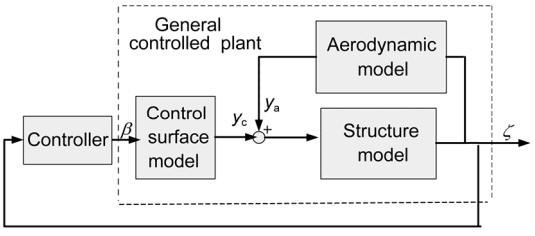

Figure 7 Closed-loop system.

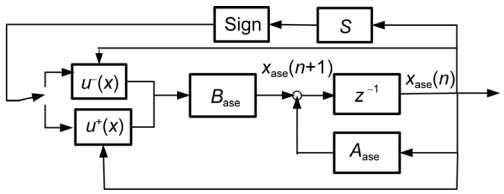

Figure 8 Control block diagram of SMC.

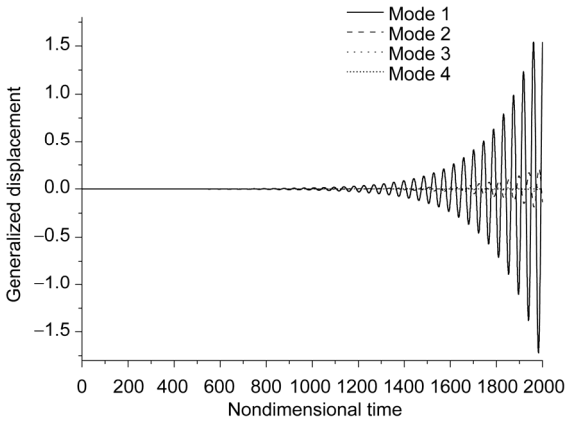

Figure 9 First four modes generalized open-loop displacement curve (at dynamic pressure $85 lbf/ft^2$).

In order to apply the SMC method to suppress the flutter as depicted by Figure 9, aiming at eq. (16) to introduce the similar transformation matrix

$$T=\begin{pmatrix} I_{n-m} & -B_{\text{ase1}}\left(B_{\text{ase2}}\right)^{-1} \\ 0 & I_m \end{pmatrix},$$

where

$$B_{\text{ase}}=\begin{pmatrix} B_{\text{ase1}} \\ B_{\text{ase2}} \end{pmatrix},\quad B_{\text{ase1}}\in R^{(n-m)\times m},\ B_{\text{ase2}}\in R^{m\times m}.$$

Let $\overline{x}_{\text{ase}}=Tx_{\text{ase}}$, eq. (16) is transformed into the standard quadratic form

$$\begin{cases} \overline{x}_{\text{ase1}}\left(n+1\right)=\overline{A}_{11}\overline{x}_{\text{ase1}}\left(n\right)+\overline{A}_{12}\overline{x}_{\text{ase2}}(n), \\ \overline{x}_{\text{ase2}}\left(n+1\right)=\overline{A}_{21}\overline{x}_{\text{ase1}}\left(n\right)+\overline{A}_{22}\overline{x}_{\text{ase2}}+B_{\text{ase2}}\beta(n), \end{cases} \tag{19}$$

where $\overline{x}_{\text{ase1}}\in R^{(n-m)}$, $\overline{x}_{\text{ase2}}\in R^{m}$, $\overline{A}=TA_{\text{ase}}T^{-1}$.

According to the controllability criterion, the system described by eq. (16), namely $(A_{\text{ase}}, B_{\text{ase}})$ is controllable. Further, we can deduce that $(\overline{A}_{11}, \overline{A}_{12})$ is controllable. The coefficient matrix S of sliding surface function can be determined by the pole placement of $(\overline{A}_{11}-\overline{A}_{12}\overline{S})$, where $\overline{S}=ST^{-1}$.

The modulus of the eigenvalues of the matrix $\overline{A}_{11}$ should be less than one to ensure the stability of the system. For the case of the flutter divergence of Figure 9, the matrix $\overline{A}_{11}$ has two unstable eigenvalues. We can assign two stable eigenvalues to $\overline{A}_{11}$ and then the feedback gain matrix $\overline{S}$ can be obtained.

The exponent approach law for SMC is adopted as described as following:

$$\sigma(k+1)-\sigma(k)=-qT\sigma(k)-\varepsilon T\,\text{sgn}(\sigma(k)), \tag{20}$$

where $\varepsilon>0,\ q>0,\ 1-qT>0$, T is the sampling time.

Therefore, the control function eq. (18) can be written as:

$$u(n)=\begin{cases} -\left(SH\right)^{-1}\left[SGx_{\text{ase}}(n)-(1-qT)\sigma(k)+\varepsilon T\right],\ \sigma>0, \\ -\left(SH\right)^{-1}\left[SGx_{\text{ase}}(n)-(1-qT)\sigma(k)-\varepsilon T\right],\ \sigma<0. \end{cases} \tag{21}$$

Here, take ε as 10 and q as 18.

Apply the SMC of eq. (21) to the open-loop system and construct the closed-loop system. The closed-loop behavior is presented in Figure 10. The control surface deflection time history is shown in Figure 11. Compared with Figure 9, the controlled variables can converge to zero rapidly. The control function could switch quickly between the two expressions of eq. (21). It should be noted here it is the switching behavior of the surface deflection shown in Figure 11 that renders the system stable.

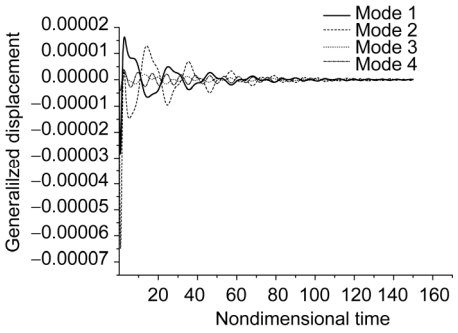

Figure 10 First four order mode closed-loop generalized displacement curve with SMC (at dynamic pressure 85*lbf/ft*^{2}).

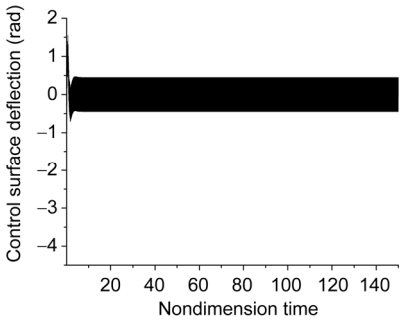

Figure 11 Control surface deflection time history with SMC.

It is possible to measure state variables when states feedback is applied. However, most state variables are difficult or are unable to be measured in practical engineering problems. Thus it is necessary to design an observer to reconstruct unmeasured state variables when the system is observable. In addition, there exist internal noise and measurement noise to the system. Considering noise, eq. (15) can be rewritten as:

$$\begin{aligned} x_{\text{ase}}\left(n+1\right)&=A_{\text{ase}}x_{\text{ase}}\left(n\right)+B_{\text{ase}}\beta(n)+G_{\text{ase}}w(n), \\ y_{\text{ase}}(n)&=C_{\text{ase}}x_{\text{ase}}\left(n\right)+v(n), \end{aligned} \tag{22}$$

where $w(n)$ denotes disturbed noise and $v(n)$ is measurement noise. They are zero-mean Gaussian noise processes (uncorrelated from each other) with power spectrum Q_N and R_N, respectively.

In the example, we deduce that eq. (22) is observable. We apply LQG method to eq. (22) to realize optimal control. Based on separation principal, the construction of LQG optimal controller can be divided two parts, which contain the optimal state-feedback controller and the optimal state-estimator.

The gain matrix of optimal state-feedback controller $\beta(n)=-R^{-1}B_{\text{ase}}{}^{\text{T}}Px_{\text{ase}}(n)$ makes the following criteria $\boldsymbol{J}$ to be the minimum

$$\boldsymbol{J}=\frac{1}{2}\sum_{n=0}^{\infty}\left[x_{\text{ase}}[n]^{\text{T}}\boldsymbol{Q}x_{\text{ase}}[n]+\beta[n]^{\text{T}}\boldsymbol{R}\beta[n]\right], \tag{23}$$

P is the unique positive-definite solution to the following Algebraic Riccati Equation:

$$PA_{\text{ase}}+A_{\text{ase}}{}^{\text{T}}P-PB_{\text{ase}}\boldsymbol{R}^{-1}B_{\text{ase}}{}^{\text{T}}P+\boldsymbol{Q}=0, \tag{24}$$

$\boldsymbol{Q}$ is the control weight matrix and $\boldsymbol{R}$ is the input weight matrix. In order to obtain better control effect, when control cost is lower, the control signal can be set relatively higher. In this condition, the input weight matrix $\boldsymbol{R}$ can be set relatively small whereas state weight matrix $\boldsymbol{Q}$ can be set large and *vice versa*. The deflection angle of control surface of AGARD445.6 wing cannot be infinitely large, so let the matrix $\boldsymbol{R}$ relatively large and the matrix $\boldsymbol{Q}$ small, here let $\boldsymbol{R}$=(1 0), $\boldsymbol{Q}=0.1\boldsymbol{I}_{4\times4}$.

Designing the Kalman filter, that is, the optimal state observer is as follows:

$$\begin{aligned}\hat{x}_{\text{ase}}(n+1)&=(A_{\text{ase}}-LC_{\text{ase}})\hat{x}_{\text{ase}}(n)\\&\quad+B_{\text{ase}}\beta(n)+Ly_{\text{ase}}(n),\end{aligned} \tag{25}$$

where $L=P_NC_{\text{ase}}{}^{\text{T}}R_N{}^{-1}$ is filter gain matrix, $\hat{x}$ the estimated states. P_N is the unique positive-definite solution to the following equation:

$$A_{\text{ase}}P_N+P_NA_{\text{ase}}{}^{\text{T}}+G_{\text{ase}}Q_NG_{\text{ase}}{}^{\text{T}}-P_NC_{\text{ase}}{}^{\text{T}}R_N{}^{-1}C_{\text{ase}}P_N=0.$$

LQG algorithm is depicted as Figure 12.

Applying LQG approach to the example, the closed-loop system generalized displacement responses and control surface deflections are shown in Figures 13 and 14, respectively. This indicates that the generalized displacement responses decay rapidly to zero steady status and the amplitude of the control surface deflection is also within the reasonable range.

Compared with LQG, SMC can stabilize the output responses of the controlled system at equilibrium state more rapidly. It should be noted that SMC can also be used in the case containing unmeasurable state variables and the related work will be done in the future.

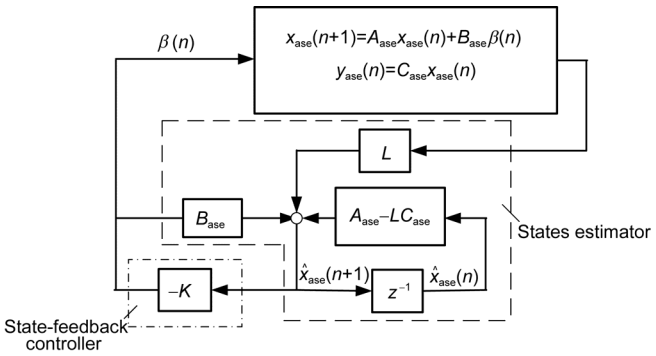

Figure 12 LQG control diagram.

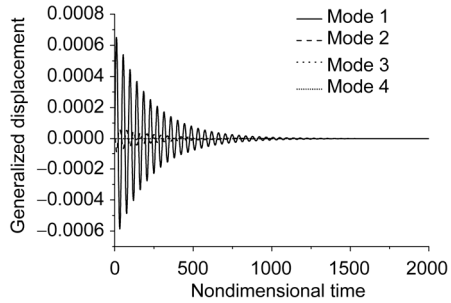

Figure 13 First four order mode closed-loop generalized displacement curve with LQG (at dynamic pressure 85*lbf/ft*^{2}).

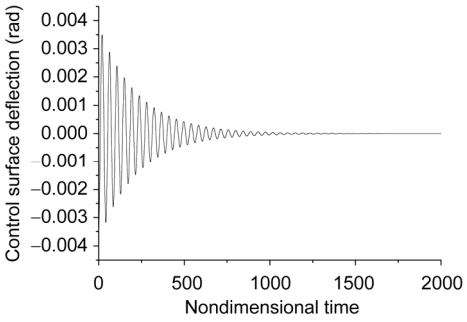

Figure 14 Control surface deflection time history with LQG.

6 Conclusions

For direct coupled CFD/CSD calculation reduces the computational efficiency and is not suitable for analyzing and designing aeroelastic problems and active flutter suppression. Thus the Volterra-based ROM technique is suggested and used to substitute CFD to calculate unsteady aerodynamic forces. ROM with a state-space model of the structure was constructed to build an open-loop aeroelastic model for the AGARD445.6 wing herein. Based on this application of SMC with state-feedback and LQG control approaches for active flutter suppression were investigated. The results show that SMC algorithm has better control effect and can suppress flutter more rapidly than the LQG method.

In the future work, we will focus on how to design SMC with state observer when state variables unmeasurable and investigate how to make the SMC more robust while the model parameters change.

1 Guruswamy G P. Vortical flow computations on swept flexible wings using navier-stokes equations. AIAA J, 1990, 28: 2077–2133
2 Lee-Rausch E M, Batina J T. Wing flutter computations using an aeroelastic model based on the navier-stokes equations. J Aircraft, 1996, 33: 1139–1147
3 Alonso J J, Jameson A. Fully-implicit time-marching aeoelastic solutions. In: Proceedings of 32nd AIAA Aerospace Sciences Meeting

and Exhibit. Reno: AIAA, 1994. AIAA 94–0056
4 Zhen G N, Yang G W, Qian W. Flutter analyses of complete aircraft based on hybrid grids and parallel computing. Sci China-Technol Sci, 2013, 56(2): 398–404
5 Lü G L, Ye Z Y. Investigation on the mechanism of aeroelastic hazard during ground test of rocket nozzle. Sci China-Technol Sci, 2012, 55(9): 2462–2473
6 Cowan T J, Andrew S, Gupta K K. Accelerating CFD-based aeroelastic predictions using system identification. J Aircraft, 2001, 38(1): 81–87
7 Munteanu S, Rajadas J, Nam C, et al. A volterra kernel reduced-order model approach for nonlinear aeroelastic analysis. In: Proceedings of 46th AIAA/ASME/ASCE/AHS/ASC Structures, Structural Dynamics and Materials Conference. Austin: AIAA, 2005. AIAA 2005-1854
8 Hall K C, Thomas J P, Dowell E H. Proper orthogonal decomposition technique for transonic unsteady aerodynamic flows. AIAA J, 2000, 38(10): 1853–1862
9 Thomas J P, Hall K C, Dowell E H. A harmonic balance approach for modeling nonlinear aeroelastic behavior of wings in transonic viscous flow. In: Proceedings of 44th AIAA/ASME/ASCE/AHS/ASC Structures, Structural Dynamics, and Materials Conference. Norfolk: AIAA, 2003. AIAA 2003-1924
10 Waszak M R, Srinathkumar S. Flutter suppression for the active flexible wing: A classical design. J Aircraft, 1995, 32(1): 61–67
11 Hodges G E. Active flutter suppression-B-52 control configured vehicle. In: Proceedings of AIAA Dynamics Specialists Conference. Williamsburg: AIAA, 1973. AIAA 73-322
12 Hwang C, Johnson E H, Pi W S. Recent development of the YF-17 active flutter suppression system. J Aircraft, 1981, 18(7): 537–545
13 Xu M, Chen G, Chen S L, et al. Design method of active control law based on reduced order model of unsteady aerodynamics for aeroelasticity (in Chinese). J Northwestern Polytech Univ, 2004, 22(6): 748–752
14 Yang G W, Zheng G N, Li G B. Computational methods and engineering applications of static/dynamic aeroelasticity based on CFD/CSD coupling solution. Sci China-Technol Sci, 2012, 55(9): 2453–2461
15 Li G B. Study on Aeroelastic Reduced Order Models and Active Flutter Suppression. Dissertation for the Doctoral Degree. Beijing: Institute of Mechanics, 2011
16 Liu X Y. Aeroelastic Research Based on Unsteady Aerodynamic Reduced Order Model. Dissertation for the Doctoral Degree. Beijing: Beijing University of Aeronautics & Astronautics, 2011. 92–96
17 Yang C, Song C, Wu Z G, et al. Application of output feedback sliding mode control to active flutter uppression of two-dimensional airfoil. Sci China-Technol Sci, 2010, 53(5): 1338–1348
18 Kim K W, Lee B, Na S, et al. Comparative analysis of control performances applied to a 3-DOFs nonlinear supersonic lifting surface. In: Proceedings of 49th AIAA/ASME/ASCE/AHS/ASC Structures, Structural Dynamics, and Materials Conference. Schaumburg: AIAA, 2008. AIAA 2008-1724
19 Na S, Marzocca P, Librescu L, et al. Sliding mode aeroelastic control of supersonic 2-D flapped lifting surfaces. In: Proceedings of 48th AIAA/ASME/ASCE/AHS/ASC Structures, Structural Dynamics, and Materials Conference. Honolulu: AIAA, 2007. AIAA2007-2349
20 Juang J N, Pappa R S. An eigensystem realization algorithm for modal parameter identification and model reduction. J Guid Control Dyn, 1985, 8: 620–627
21 Volterraa V. Theory of Functionals and of Integral and Integrao-differential Equation. New York: Dover Publications, 1959
22 Silva W A. Discrete-Time Linear and Nonlinear Aerodynamic Impulse Responses for Efficient CFD Analysis. Dissertation for the Doctoral Degree. Williamsburg: College of William & Mary, 1997
23 Silva W A. Reduced-order models based on linear and nonlinear aerodynamic impulse response. In: Proceedings of the 40th AIAA/ASE/ASCE/AHS/ASC Structures, Structural Dynamics, and Materials Conference, St. Louis: AIAA, 1999
24 Raveh D E. Reduced order models for nonlinear unsteady aerodynamics. AIAA J, 2011, 39(8): 1417–1429
25 Yang G W. Recent progress on computational aeroelasticity (in Chinese). Adv Mech, 2009, 39(4): 406–420
26 Yates E C. Agard standard aeroelastic configurations for dynamic response I-wing 445.6. In: Proceedings of 61st Meeting of the Structures and Materials Panel at Oberammergau. Germany: Neuilly-sur-Seine, 1985